Journal of Materials Chemistry A

Accepted Manuscript

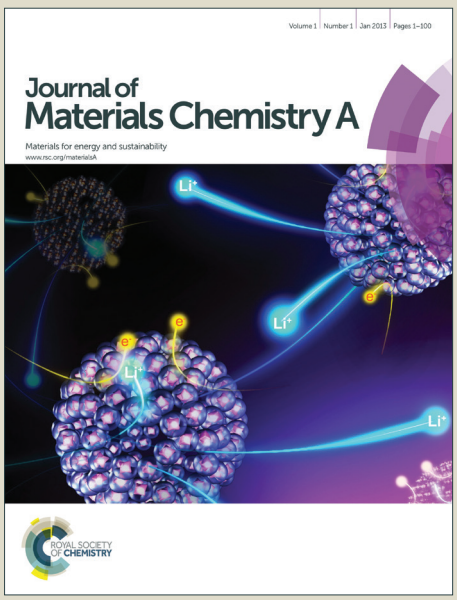

ROYAL SOCIETY OF CHEMISTRY

www.rsc.org/materialsA

Cite this: DOI: 10.1039/c0xx00000x

www.rsc.org/xxxxxx

ARTICLE TYPE

Effects of LnF_3 on reversible and cyclic hydrogen sorption behaviors in $NaBH_4$: Electronic nature of Ln versus crystallographic factors

Lina Chong,[a] Jianxin Zou,*[a,b] Xiaoqin Zeng [a,b] and Wenjiang Ding [a,b]

Received (in XXX, XXX) XthXXXXXXXXX 20XX, Accepted Xth XXXXXXXXX 20XX

DOI: 10.1039/b000000x

In the present work, the hydrogen sorption behaviors of some $3NaBH_4$-LnF_3 (Ln = Ce, Sm, Gd and Yb) composites were investigated and the mechanisms associated with different effects of LnF_3 (Ln = La, Ce, Pr, Nd, Sm, Gd, Ho, Er and Yb) on the reversible hydrogen sorption in $NaBH_4$ were proposed based on careful comparisons. The key factors controlling the properties of $3NaBH_4$-LnF_3 can be summarized as follows: i) The electronegativity χ_p of the Ln^{3+} determines the thermodynamic stability of $3NaBH_4$-LnF_3 composites with χ_p lying in the range 1.23 ~ 1.54 being suitable for reversible hydrogen storage; ii) The electron configuration of Ln^{3+} influences the rehydrogenation behaviors: the more stable the oxidation state of the Ln^{3+} is, the better the rehydrogenation performance is in $NaBH_4$; iii) The unique crystal structure of Ln-B phase formed during dehydrogenation, and geometrical configuration of B in Ln-B, provide dangling bonds for hydrogen atoms to embed in, consequently modify the rehydrogenation kinetics. Since Gd^{3+} possesses the combination of suitable electronegativity, stable oxidation state and favorable geometric structure of GdB_4, the $3NaBH_4$-GdF_3 composite exhibits the best overall hydrogen storage properties among all the studied $3NaBH_4$-LnF_3 composites, with high cycling stability up to 51 cycles and fast kinetics. This understanding provides us with criterions to design new borohydride-based hydrogen storage systems and optimize their hydrogen storage properties.

1. Introduction

Hydrogen is regarded as one of the most promising clean energy resources for replacing fossil fuels. However, the storage of hydrogen is becoming the most crucial problem to the implementation of hydrogen energy.[1] Apart from the classical techniques, such as high pressure storage and cryogenics storage, a well-investigated alternative approach is the chemical hydrogen storage in solid-state form. Complex hydrides, such as metal borohydrides, imides and alanates, are considered as promising solid-state hydrogen storage materials due to their high gravimetric and volumetric hydrogen density.[2, 3] To meet the requirements for proton exchange membrane fuel cells, the hydrogen storage systems must desorb hydrogen at temperatures below 300 °C, and be reversible under moderate conditions. These conditions restrict the flexibility of dehydrogenation enthalpies of the hydrogen storage systems in the range of 30 ~ 60 kJ mol^{-1} H_2, estimated for the reversible H_2 storage materials.[4]

$NaBH_4$, for instance, has a high gravimetric capacity of 10.8 wt%, high volumetric hydrogen density of 113 kg m^{-3} H_2, and low cost along with good stability to air exposure, fulfilling some of the basic requirements for onboard hydrogen storage set by the US Department of Energy (DOE).[5] The full dehydrogenation of $NaBH_4$ takes place as:

$$NaBH_4 \rightarrow Na + B + 2H_2\ (g) \quad (1).$$

The decomposition enthalpy of $NaBH_4$ is 108 ± 3 kJ mol^{-1} H_2,[6] which means that the dehydrogenation of $NaBH_4$ only occurs at about 534 ± 10 °C at 1 bar H_2.[6] It is too high to be used for practical applications. Moreover, the reversibility of $NaBH_4$ alone cannot be achieved.[7] To overcome the drawbacks mentioned above, extensive efforts have been devoted to improve the hydrogen sorption thermodynamics, kinetics and reversibility of $NaBH_4$.

Recently, Nakamori et al.[8] proposed that the formation enthalpy of metal borohydride $M(BH_4)_n$ (M = metal, n depending on valence of the metal) displays an intrinsic correlation with the Pauling electronegativity (χ_p) of the metal cation, showing that the dehydrogenation temperature of the $M(BH_4)_n$ decreases with increasing the χ_p of the metal cation. Such finding opens up a possible way to destabilize $NaBH_4$, that is, the partial substitution of Na^+ by other cations having higher χ_p may be effective for lowering down the hydrogen desorption temperature of $NaBH_4$. Such a speculation has been realized in cation substitution in $NaBH_4$ through synthesizing double or multi-cation borohydrides, *e.g.* $NaZn_2(BH_4)_5$ and $NaZn(BH_4)_3$, and the decomposition temperatures of these multi-cation borohydrides are far lower than that of pure $NaBH_4$.[9,10] Unfortunately, no reversibility can be obtained in those multi-cation borohydrides. Finding out the suitable electronegativity of the added metal cation is essential for exploring hydrogen carriers with appropriate stability and reversibility for practical applications.

Another approach is nano-crystallization or nano-confinement. Incorporating $NaBH_4$ into nanoporous scaffolds to produce nano-

[a]*National Engineering Research Center of Light Alloys Net Forming & State KeyLaboratory of Metal Matrix Composite, Shanghai Jiao Tong University, Shanghai200240, China. E-mail: zoujx@sjtu.edu.cn; Fax: +86-21-34203730; Tel: +86-21-54742381*

[b]*Shanghai Engineering Research Center of Magnesium Materials, Application & School of Materials Science and Engineering, Shanghai JiaoTong University, Shanghai 200240, China*

† Electronic supplementary information (ESI) available.

scale $NaBH_4$ particles can shorten the hydrogen diffusion lengths and increase the active surface areas, thereby, promotes hydrogen desorption kinetics.[11] However, nano-confinement reduces the hydrogen storage capacity due to the low loading rate. Catalyst doping is an alternative way to tailor the hydrogen sorption properties of $NaBH_4$.[12] Despite enhancement in hydrogen desorption performance was demonstrated in Ti-based catalysts doped $NaBH_4$, the recharging was performed under 5.5 MPa at 500 ^oC, which was still far from requirements for the on-board hydrogen storage.[12] More recently, the concept "destabilization" was proposed and successfully exemplified in the $2LiBH_4$-MgH_2 system.[13] Indeed, the addition of MgH_2 as a destabilizing reactant changed the reaction pathway and thereby reduced the overall dehydrogenation enthalpy by 25 kJ mol^{-1} H_2.[13] More importantly, the reversibility was achieved under moderate conditions. It turns out that the decrease in dehydrogenation enthalpy and the facilitating in rehydrogenation reaction are attributed to the formation of MgB_2 in which the Mg-B bonds are relatively weaker than B-B bonds in boron.[7] Similar to the role of MgB_2, AlB_2 in recovering $LiBH_4$ has also been successfully demonstrated.[14]

Searching for reactive agents which not only reduce thermodynamic stability but also maintain a high cycling life for $NaBH_4$ is a great challenge and an essential target. Motivated by this, in our previous work, we have synthesized several reversible hydrogen storage systems via combining $NaBH_4$ with destabilizing agents on the basis of lanthanide metals, such as La, Nd, Pr and Ho. These systems, though had reversible hydrogen sorption capacities less than 4 wt%, showed fast dehydrogenation rates at low temperatures and excellent rehydrogenation properties under moderate conditions that could not be achieved in pristine $NaBH_4$.[15-18] The key feature of the thermodynamically preferred reactions is the formation of metal boride phase, which not only stabilizes the dehydrogenation products, but also allows the regeneration of borohydride taking place under mild conditions. Since lanthanide metals have remarkable self-binding abilities with born,[19] additional with the very similar chemical properties of their trivalent cations due to their similar outer and sub-outer electron configurations, the dehydrogenation of $NaBH_4$ could be modified by combining it with other lanthanide trifluorides so as to form lanthanide boride compounds upon dehydrogenation and the reversible hydrogen storage systems may be achieved. Moreover, it has been demonstrated recently that lanthanide based additives are effective in decreasing the dehydrogenation temperature of $LiBH_4$.[20, 21]

Encouraged by the above, 4 new reversible hydrogen storage systems: $3NaBH_4$-CeF_3, $3NaBH_4$-SmF_3, $3NaBH_4$-GdF_3 and $3NaBH_4$-YbF_3 were prepared through ball milling in the present work. The aim is to find out the factors governing the thermodynamic and kinetic properties of the $3NaBH_4$-LnF_3 (Ln = La, Ce, Pr, Nd, Sm, Gd, Ho, Er and Yb) systems. Systematical investigations are carried out via considering the electron configurations and electronegativities of Ln^{3+} cations as well as the crystal structures of Ln-B phases on the hydrogen sorption behaviors of $NaBH_4$. This study will be a potential indicator for exploring borohydride-based hydrogen storage systems with low operating temperatures, fast de-/rehydrogenation kinetics and good cyclic stability for practical applications.

2. Experimental

Commercial $NaBH_4$ (98%) powders were purchased from Strem Chemicals Inc. All CeF_3 (99.9%), SmF_3 (99.99%), and GdF_3 (99.99%) were obtained from Alfa Aesar. YbF_3 (99.99%) was obtained from Aladdin Chemistry Co. Ltd. All of these materials were used as received states without further purification. The sample storage and handling were manipulated in a Lab 2000 glove box (Etelux Intertgas system Co., Ltd.) filled with purified argon and equipped with recirculation system to keep both water and oxygen concentrations below 1 ppm. Samples of $3NaBH_4$-CeF_3, $3NaBH_4$-SmF_3, $3NaBH_4$-GdF_3 and $3NaBH_4$-YbF_3 (mole ratio) were prepared by mechanical ball milling under Ar atmosphere for 16 h using a QM-1SP2 planetary ball mill at 456 rpm in a stainless steel vessel. The stainless steel vessel for ball milling was 100 ml, and the weight ratio of the sample to the ball was 1:30.

The hydriding/dehydriding properties were measured in a Sievert type pressure-composition-temperature (PCT) apparatus manufactured by Shanghai Institute of Microsystem and Information Technology. Temperature-programmed-dehydrogenation (TPD) curves were determined by volumetric methods, starting from vacuum with the temperature increased from ambient to about ~ 463 ^oC at a constant heating rate of 3 ^oC min^{-1}. The PCT measurements were performed at different temperatures in the hydrogen pressure range of 0.0019 ~ 4.6 MPa after the sample being completely dehydrogenated. For the hydrogen absorption cycling tests, the sample was directly pressurized with hydrogen at the desired temperature after completely dehydrogenated. Isothermal dehydrogenation cycling tests were performed at 400 ^oC for 2 h in static vacuum. Approximately ~ 3.0 g of sample was used for PCT measurements, 150 mg for isothermal de-/rehydrogenation kinetic and cycling measurements, and 100 mg for TPD measurements. For an evaluation of the practical hydrogen storage property, the hydrogen-storage capacity of each sample was calculated based on their original total weight including $NaBH_4$ and LnF_3 (Ln = Ce, Sm, Gd, Yb).

Thermogravimetry (TG) and differential scanning calorimetry (DSC) analyses were carried out using synchronous thermal analyzer (TG/DSC, Netzsch, STA 449 F3 Jupiter). The heating rate was set at 3, 5 and 10 K min^{-1}, respectively, under 1 bar flowing argon atmosphere with the temperature rising from 26 to 500 ^oC. About 10 mg of sample was used each time.

Phase components of samples in ball milled, dehydrogenated and rehydrogenated states were identified by X-ray diffraction (XRD Rigaku D/MAX-2500, VL/PCX, Cu Kα radiation) from 10^o to 90^o (2θ) with a step width of 0.02^o. To avoid the oxidation during the XRD measurements, sample powders were flattened into a container and covered by a scotch in the Ar filled glove box. Chemical bonding analyses were examined by Fourier transform infrared spectroscopy (FT-IR, Nicolet iS5, Thermo Fisher Scientific Inc. U.S.A.) equipped with a horizontal ATR accessory (Germanium crystal) in an argon-filled glovebox.

3. Results and discussions

3.1 Hydrogen release and uptake behaviors

The effects of CeF_3, SmF_3, GdF_3 and YbF_3 on the 1st hydrogen

desorption behaviors of $NaBH_4$ in the temperature range 30 ~ 463 °C are evaluated by using TPD (Fig. S1(a)). Evidently, the onset dehydrogenation temperatures of $NaBH_4$ in CeF_3, SmF_3, GdF_3 and YbF_3 containing composites are measured to be around 150, 212, 112 and 156 °C, and the maximum dehydrogenation rates are obtained at 412, 422, 409 and 440 °C, respectively. To complete the dehydrogenation at 463 °C, about 0.3 h is needed for $3NaBH_4$-CeF_3, $3NaBH_4$-SmF_3 and $3NaBH_4$-YbF_3 composites, while only 0.1 h is required for $3NaBH_4$-GdF_3 composite. Finally, 3.49, 3.47, 3.50 and 3.23 wt% of H_2 are released from $3NaBH_4$-CeF_3, $3NaBH_4$-SmF_3 $3NaBH_4$-GdF_3 and $3NaBH_4$-YbF_3 composites, respectively, fairly close to their corresponding theoretical values (3.54, 3.58, 3.51 and 3.31 wt%, respectively).

Furthermore, the apparent activation energies (E_a) of the four composites are determined using the Kissinger's approach,[22] as described below:

$$\frac{d\left(\ln\frac{\beta}{T_m^2}\right)}{d\left(\frac{1}{T_m}\right)} = -\frac{E_a}{R} \quad (2),$$

where β, T_m and R are the heating rate, the absolute temperature for the maximum desorption rate and the gas constant, respectively. In the present work, T_m is obtained from the non-isothermal dehydrogenation curves conducted by TG/DSC measurements at various heating rates (Fig. 1, data shown in Table S1). The dependence of $\ln(\beta/T_m^2)$ on $1/T_m$ is plotted (Fig. S2(a)), displaying the good linear relationships for all the four composites, and the E_a value of each composite is calculated (data given in Table S2). In addition, TG curves evidence the close amount of the released hydrogen to their corresponding values determined by TPD (Table S1).

Subsequently, the onset dehydrogenation temperatures - T_{on}, peak temperatures -T_p and E_a of $3NaBH_4$-LnF_3 (Ln = La, Ce, Pr, Nd, Sm, Gd, Ho, Er and Yb) composites as a function of trivalent Ln, are plotted to systematically clarify the effects of the LnF_3 on hydrogen release behaviors in $NaBH_4$ (Fig. 2, data collected in Table S2). T_{on}, T_p and E_a data of $3NaBH_4$-ErF_3 composite, and E_a of $3NaBH_4$-NdF_3 composite are obtained according to Fig. S1(b) and S2(b, c). Interestingly, it is found that the T_{on}, T_p and E_a of $3NaBH_4$-LnF_3 composites show a gradual decrease from La^{3+} to Nd^{3+}, Sm^{3+} to Gd^{3+}, and Ho^{3+} to Er^{3+}, respectively. Such a

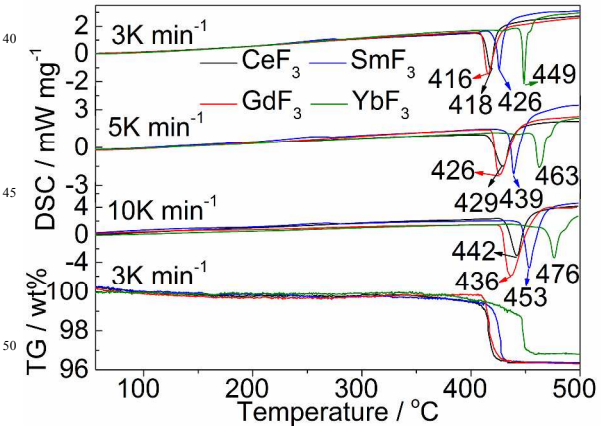

Fig. 1 DSC curves (heating rate 3, 5 and 10 K min^{-1}) and TG curves (heating rate 3 K min^{-1}) of the $3NaBH_4$-CeF_3, $3NaBH_4$-SmF_3, $3NaBH_4$-GdF_3 and $3NaBH_4$-YbF_3 composites under 1 bar argon atmosphere.

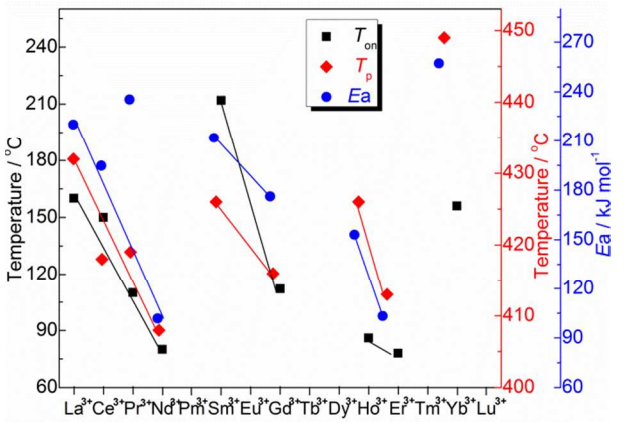

Fig. 2 Relations between the onset dehydrogenation temperature-T_{on} (black square), peak temperature-T_p (red rhombus), E_a (blue circle) of $3NaBH_4$-LnF_3 (Ln = La, Ce, Pr, Nd, Sm, Gd, Ho, Er and Yb) composites and trivalent Ln, respectively.

phenomenon can be understood considering the so called "Lanthanide Tetrad Effect", which is originated from the disturbance of coherent periodic filling of the *f* sub-shell of the electron configuration of trivalent lanthanides in four groups: La^{3+} – Nd^{3+}, Pm^{3+} – Gd^{3+}, Tb^{3+} – Er^{3+} and Tm^{3+} – Lu^{3+}.[23] Therefore, the effect of LnF_3 on the dehydrogenation performance of $NaBH_4$ is actually related to the *f* shell electron configuration of the Ln^{3+}cation.

By integrating the peak areas in DSC profiles, the dehydrogenation enthalpies of $3NaBH_4$-CeF_3, $3NaBH_4$-SmF_3, $3NaBH_4$-GdF_3 and $3NaBH_4$-YbF_3 composites are verified to be 46.3, 47.6, 63.1 and 43.8 kJ mol^{-1} H_2, respectively, which show reductions of 41.6 ~ 59.4% compared to that of $NaBH_4$ alone (108 ± 3 kJ mol^{-1} of H_2),[6] verifying the considerable decrease in dehydrogenation enthalpy of $NaBH_4$ through the LnF_3 addition. Moreover, these results fall in the range of 30 ~ 60 kJ mol^{-1} H_2 estimated for the reversible storage materials, implying the reversibilities of the four composites which are corroborated by the PC isotherms measurements (Fig. 3). Obviously, in the case of $3NaBH_4$-CeF_3, $3NaBH_4$-SmF_3 and $3NaBH_4$-YbF_3 composites (Fig. 3-up), reversible capacities of 1.52, 1.90 and 1.45 wt% are obtained with sloping absorption/desorption plateaus under 4.5 MPa, respectively. Remarkably, the $3NaBH_4$-GdF_3 composite exhibits the highest reversible hydrogen-storage capacity with stable and flat absorption/desorption plateaus (Fig. 3-down), indicating that the $3NaBH_4$-GdF_3 composite has the best hydrogen storage kinetics and reversibility among the four composites. Table 1 summarizes the data corresponding to Fig. 3-down. In contrast, regeneration of $NaBH_4$ from its decomposition products (NaH + B) under 350 bar hydrogen pressure at 400 °C for 24 h was unsuccessful.[7]

3.2 Relationship of de-/rehydrogenation mechanisms and the crystal structures of Ln-B phases

For investigation of the hydrogen sorption mechanisms, the phases in the four composites after ball milling, dehydrogenation and rehydrogenation are characterized by XRD, in tandem with FTIR. For the ball-milled $3NaBH_4$-GdF_3 composite, XRD pattern (Fig. 4, line A) proves that no new phases formed after ball

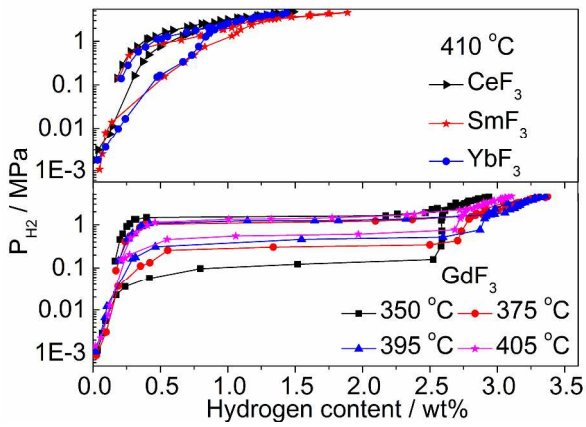

Fig. 3 PCT curves of the $3NaBH_4$-CeF_3, $3NaBH_4$-SmF_3 and $3NaBH_4$-YbF_3 composites measured at 410 °C, as well as $3NaBH_4$-GdF_3 composite measured at 350, 375, 395 and 405 °C.

Table 1 PCT data of $3NaBH_4$-GdF_3 composite at different temperatures. Data for pure $NaBH_4$[6] are given as a reference.

sample	T / °C	Rehyd. P / MPa	Dehyd. P / MPa	Reversible H_2 capacity / wt%
	350	1.56	0.11	2.94
$3NaBH_4$-GdF_3	375	1.17	0.33	3.38
	395	1.26	0.47	3.36
	405	1.33	0.55	3.11
Pure $NaBH_4$	684	35 (400 °C)[7]	0.96	irreversible

milling except for $NaBH_4$ and GdF_3. In contrast, the formations of bimetallic borohydride chlorides or lanthanide borohydrides were observed in the ball milled $LiBH_4$-$LnCl_3$ and $NaBH_4$-$LnCl_3$ systems.[20, 21, 24] The characteristic peaks of B-H bonds of $NaBH_4$ are further revealed in the FTIR spectra (Fig. S3(a)). However, after complete dehydrogenation (Fig. 4, line B), new compounds, NaF, GdB_4 and GdH_2, instead of the original ones appear, indicating that the observed hydrogen desorption corresponds to the dehydrogenation reaction between $NaBH_4$ and GdF_3. FTIR result further confirms the complete decomposition of $NaBH_4$ by showing the disappearance of the B-H bonds of $NaBH_4$ after dehydrogenation (Fig. S3(b)). Based on XRD and FTIR results, the main dehydrogenation reaction pathway of the $3NaBH_4$-GdF_3 composite can be therefore described as follows:

$$12NaBH_4 + 4GdF_3 = 12NaF + 3GdB_4 + GdH_2 + 23H_2(g) \quad (3).$$

XRD, FTIR results combined with calculation by using HSC Chemistry program (Fig. S5)[25] evidence the similar dehydrogenation pathways in the $3NaBH_4$-LnF_3 (Ln = Ce, Sm and Yb) composites (Fig. S4): during dehydrogenation processes, $NaBH_4$ reacts with LnF_3 to yield NaF, Ln-B and Ln-H phases. The formations of Ln-B and Ln-H (Ln = La, Ce, Pr, Nd, Sm, Gd, Ho, Er or Yb) were also demonstrated in the dehydrogenated $LiBH_4$-$LnCl_3$[20, 21] and $NaBH_4$-LnF_3 systems.[15-18]

After hydrogen absorption (Fig. 4, line C), the characteristic peaks assigned to $NaBH_4$ are clearly observed. To clarify this, FTIR investigation was carried out and further confirmed the regeneration of $NaBH_4$ (Fig. S3(c)). Moreover, the diffraction peaks from NaF, GdB_4 and GdH_2 phases disappear along with the appearance of GdF_3. These results imply that NaF, GdB_4 and GdH_2 take part in the rehydrogenation reaction to yield $NaBH_4$ and GdF_3 during H_2 uptake process. In addition, $NaGdF_4$ is also detected in the case of $3NaBH_4$-GdF_3 composite. According to XRD and FTIR analyses, the rehydrogenation pathway in $3NaBH_4$-GdF_3 composite can be proposed as follows:

$$12NaF + 3GdB_4 + GdH_2 + 23H_2(g) = 12NaBH_4 + 4GdF_3 \quad (4),$$

together with a side reaction:

$$NaF + GdF_3 = NaGdF_4 \quad (5);$$

A similar rehydrogenation mechanism was reported in the study of $3NaBH_4$-NdF_3 system.[15] The analogous H_2 uptake pathways also exist in $3NaBH_4$-LnF_3 (Ln = Ce, Sm and Yb) composites, as illustrated in Fig. S3 and S4. More detailed discussions about the de-/rehydrogenation reactions in $3NaBH_4$-LnF_3 (Ln = Ce, Sm and Yb) composites are displayed in the supplementary information. It is worth noting here that a better hydrogen storage performance, especially the reversibility, is found in $NaBH_4$-LnF_3 systems than that in corresponding $NaBH_4$-$LnCl_3$ ones.[24] Such a phenomenon is mainly attributed to the substitution of F^- for H^- in $NaBH_4$-LnF_3 systems, which leads to a favorable modification of hydrogen sorption thermodynamics in these systems.[26]

Besides the lower energy needed to break the bond of Ln-B contributing to the thermodynamic regeneration of $NaBH_4$, it is interesting to note that the crystal structure of Ln-B phase should be also of great importance facilitating the recombination of $NaBH_4$. LaB_6, CeB_6, PrB_6 and NdB_6 exhibit cubic structure with a space group of *Pm*-3*m* (221), while SmB_4, GdB_4, HoB_4, ErB_4 and YbB_4 have the tetragonal *P*4/*mbm* (127) structure. As illustrated in Fig. S6(a)(I) and (II), B appears in the form of B_6 octahedron configuration in either LnB_6 or LnB_4 phases, which offers dangling bond for hydrogen atoms to embed in. Taking LaB_6 for example, it is reported that LaB_6 displays potential in promoting the hydrogen equilibrium due to the catalytic effect from La for hydrogen sorption[27] and the special crystal structure of LaB_6. The thermodynamically stable (001) plane of LaB_6 presumably contains lattice imperfections, such as vacancies, which are responsible for the catalytic behaviors.[27] The unsaturated dangling bonds in the vacancies might be used for trapping hydrogen atoms, which occurs on the boron atoms at each corner as well as the upper layer of the vacancy. Furthermore, the top layer of the LaB_6 (111) surface is composed of the triangular faces of B_6 octahedron, and in forming the

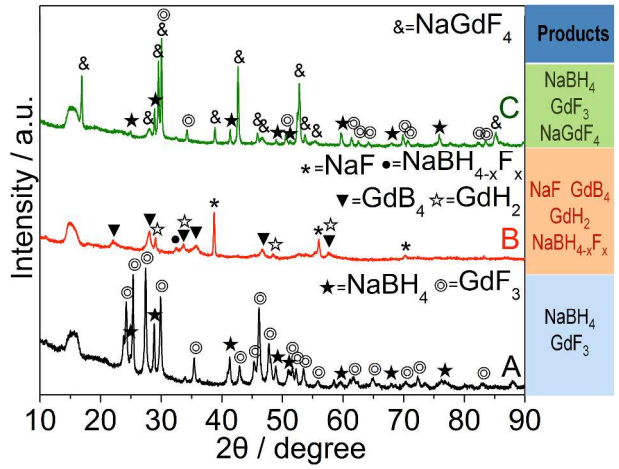

Fig. 4 XRD patterns of the (A) as-prepared; (B) dehydrogenated; (C) rehydrogenated $3NaBH_4$-GdF_3 composite.

surface, the inter-octahedral bonds are broken, resulting in three dangling bonds being 55° from normal along three azimuths 120° apart (seen in Fig. S6(b)), whereas on the (100) surface leading to a single boron dangling bond oriented along the surface normal through the middle of a square of four lanthanum atoms.[28] This allows the hydrogen atoms easily access to those active sites on LaB_6.[28] Moreover, as shown in Fig. S6(a)(I) and (II), the LnB_6 (Ln = La, Ce, Pr and Nd) and LnB_4 (Ln = Sm, Gd, Ho, Er and Yb) exhibit the same structure on either (100) or (010) surfaces. Due to the same B_6 octahedron configuration and the analogous chemical properties of lanthanide series, it is believed that LnB_6 and LnB_4 exist similar promoting effect on the rehydrogenation kinetics of $NaBH_4$. In comparison to the configuration of B atoms in LnB_x (x = 4 or 6), the crystal structure of $NaBH_4$ is shown in Fig. S6(a)(III), in which B in the $[BH_4]^-$ ligand possesses also the octahedral arrangement. Therefore, the configuration of B in either LnB_6 or LnB_4 phase may offer a possible entrance to facilitate the recombination of $[BH_4]^-$, and thereby enhances the hydrogen absorption kinetics. The crystal structures of those well-known metal borides, such as TiB_2, MgB_2, AlB_2 and CaB_6 having promotion effects on the regeneration of borohydrides are also displayed here for comparison. TiB_2, MgB_2 and AlB_2 typically crystallize in the AlB_2-type structure (hexagonal, p6/mmm) (Fig. S6(c)(I)), where the coplanar graphite-like B layers are present alternatively with the close-packed metal sheets. It was suggested that MgB_2 promoted the formation of $[BH_4]^-$ ligand, and thus enabled the regeneration of $NaBH_4$.[7] We have studied the reversibility of $2NaBH_4$-MgF_2 system. It was found that after complete dehydrogenation at 576 °C, MgB_2 was detected by XRD. However, only 0.6 wt% hydrogen was absorbed during the PCT measurement at 430 °C. In the case of CaB_6 (Fig. S6(c)(II)), though it is also cubic type with B in the form of B_6-octahedrons located at the corners of the cube, Ca atoms are inserted into a network of boron cages and the covalent bonding between B atoms is very strong, thus the spin splitting of the defect level of the B-antisite is too small to offer enough sites for H.[29] Table S3 presents the conditions needed for TiB_2, MgB_2, AlB_2, CaB_6 and Ln-B to regenerate borohydrides. As can be seen, the fastest hydrogen absorption kinetics for the regeneration of borohydrides without any catalyst addition is achieved in systems containing Ln-B phases. These results imply the remarkable contribution of the crystal structure of Ln-B phase to the rehydrogenation kinetics of $NaBH_4$.

3.3 Relationship between the enthalpy change (ΔH) and the electronegativity (χ_p) of lanthanide trivalent cation

Electronegativity (χ_p) of Ln^{3+} has been considered for further elucidating the significant enhancement of LnF_3 in destabilization and regeneration of $NaBH_4$, since χ_p of the added metal cation may influence the stability of borohydride. In Fig. 5, the de-/rehydrogenation enthalpies (ΔH_d / ΔH_f) of $3NaBH_4$-LnF_3 (Ln = La, Ce, Pr, Nd, Sm, Gd, Ho, Er andYb) composites, as a function of χ_p of Ln^{3+}cation, are plotted (data given in Table S4). The ΔH_f of the $3NaBH_4$-GdF_3 and $3NaBH_4$-ErF_3 composites were calculated according to Fig. S7, while the ΔH_f of $3NaBH_4$-CeF_3, $3NaBH_4$-SmF_3 and $3NaBH_4$-YbF_3 cannot be obtained by PCT measurements due to the unachievable rehydrogenation equilibrium.

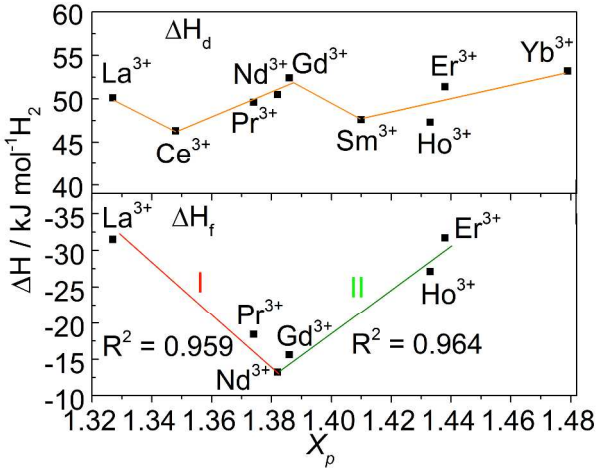

Fig. 5 Relationships between the dehydrogenation (up)/rehydrogenation (down) enthalpies (ΔH_d/ΔH_f) and the electronegativities (χ_p) of Ln^{3+} cations.

Fig. 5-up displays a W-type relationship between ΔH_d of $3NaBH_4$-LnF_3 and χ_p of Ln^{3+}, which is somewhat analogous to the relationship between Ln^{3+} and their electron configurations existing in a W-type tetrad effect.[23] It is worth noting that a V-type relationship between the ΔH_f of $3NaBH_4$-LnF_3 and χ_p of Ln^{3+} is found which results from the changes of Ln oxidation states in the dehydrogenated products, and can be described using two lines with the intersection point at Nd^{3+}(Fig. 5-down). The first group of elements (I) includes La^{3+}, Pr^{3+} and Nd^{3+}, and the second one (II) includes Nd^{3+}, Gd^{3+}, Ho^{3+} and Er^{3+}. The linear relations can be written as the following expressions:

$\Delta H_f = 314.04\chi_p - 448.45$ (14), for the first group (I);

$\Delta H_f = -295.13\chi_p + 394.15$ (15), for the second group (II), in the unit of kJ mol^{-1} H_2.

In this respect, it is expected that $NaBH_4$ based composites with the added metal cations having χ_p approximately lying in the range 1.23 ~ 1.54 are thermodynamically preferred. In addition, it implies that the added cation plays a crucial role in improving the rehydrogenation property of $NaBH_4$. This result is not only valuable for Ln cations, but also for other metal cations. For instance, in the studies of $LiBH_4$-MgH_2/Al/TiF_3/YH_3, NaH-MgB_2, and $NaBH_4$-TiF_3/YF_3/$NiCl_2$ systems,[7, 12, 30-34] the regeneration of $LiBH_4$/$NaBH_4$ has been successfully achieved, since the χ_p values of Mg^{2+}, Al^{3+}, Y^{3+}, Ti^{3+} and Ni^{2+} are all lying in 1.23 ~ 1.54.[35] It should be point out that the stability of Ln oxidation state is another factor affecting the rehydrogenation performance of $NaBH_4$. For example, La^{3+}, Gd^{3+} and Lu^{3+} have stable electron configuations: La^{3+} (f^0), Gd^{3+} (f^7) and Lu^{3+} (f^{14}). The nearby Ln^{3+} around these three ions are inclined to change their states according to the environments. Clearly, the better H_2-absorption performances are obtained in La^{3+} and Gd^{3+} added composites compared to other $NaBH_4$ based composites with Ln having anomalous oxidation states (*e.g.* Ce^{3+}). Therefore, the cation electronegativity as well as its stability can be considered as guiding factors for reasonably design and synthesize of a novel complex hydride-based hydrogen storage system with good reversibility, superior kinetic and thermodynamic properties. The W-type and V-type relationships between de-/rehydrogenation enthalpies and Ln^{3+} are also found (Fig. S8), in consistent with

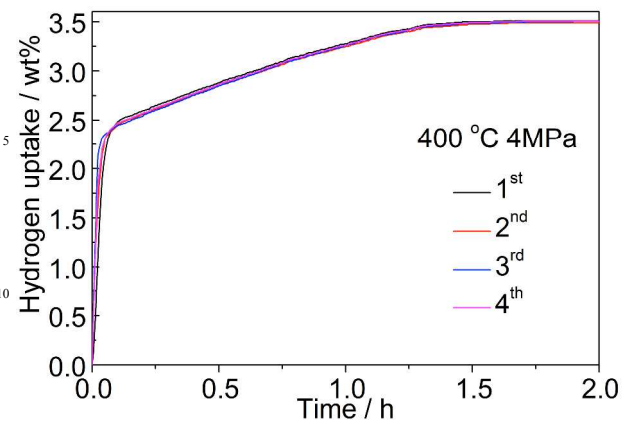

Fig. 6 Rehydrogenation curves of the $3NaBH_4$-GdF_3 composite at 400 °C under 4 MPa hydrogen pressure.

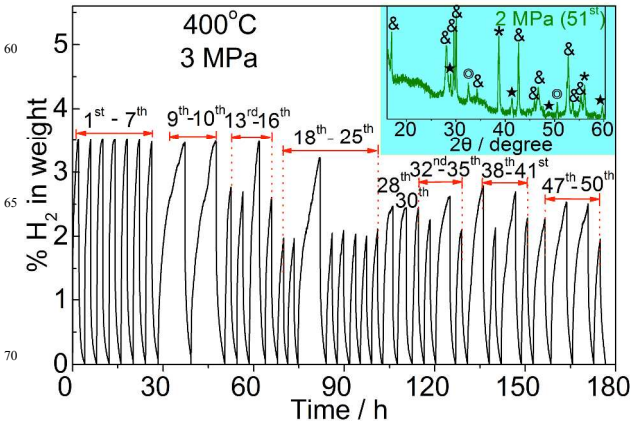

Fig. 7 Cyclic hydrogen absorption/desorption curves of the $3NaBH_4$-GdF_3 composite under constant condition – 400 °C, 3 MPa. Inset shows the XRD pattern of the rehydrogenated sample after the 51st cycle: ★ = $NaBH_4$; & = $NaGdF_4$; ⁎ = NaF; ◎ = GdF_3.

the result obtained from Fig. 5, since χ_p value of Ln cation is the reflection of its 4*f* electron properties.

3.4 Re-/dehydrogenation cycling behaviors of the $3NaBH_4$-GdF_3 composite

The cycling property of $3NaBH_4$-GdF_3 composite is investigated, since it possesses the best overall rehydrogenation performance among all the studied $3NaBH_4$-LnF_3 composites of which hydrogen storage properties are represented in Table S5 for comparison. Fig. 6 shows the rehydrogenation curves of $3NaBH_4$-GdF_3 composite at 400 °C under 4 MPa hydrogen pressure over 4 cycles. As can be seen, the H_2-absorption curves are essentially unchanged, demonstrating the excellent cyclic stability of the $3NaBH_4$-GdF_3 composite. Also, the rehydrogenation kinetics is much more pronounced. Only 4 min is required to reach about 2.40 wt% storage capacity (7.38 wt% in $NaBH_4$). After prolonging the recharging time to ~ 1.5 h, a total hydrogen capacity of 3.50 wt% is achieved. Thus, it absorbs 99.6% of the theoretical value of $NaBH_4$. In contrast, most $NaBH_4$, $LiBH_4$ or $Ca(BH_4)_2$-based hydrogen storage systems show only 43 % ~ 55 % reversibility for the 1st rehydrogenation in 5 ~ 20 h.[11, 30, 36]

Fig. 7 shows the cyclic capability of $3NaBH_4$-GdF_3 composite under 3 MPa H_2 for different cycles during a 51-cycle test. Between the cycles shown here, samples were rehydrogenated under lower temperature and pressure conditions (Data summarized in Table S6). It is notable that the $3NaBH_4$-GdF_3 composite exhibits a nearly theoretical H_2-storage capacity (3.50 wt% overall) which persists well throughout the first seven cycles even under 3 MPa H_2 pressure. However, capacity degradation appears after undergoing low temperature or pressure rehydrogenation, *i.e.* for the same rehydrogenation time of 2 h, the first absorption capacity reaches 3.50 wt%, whereas, the 50th is 1.96 wt%. A more detailed analysis of the rehydrogenation curves is shown in Fig. S9(a). XRD pattern of the rehydrogenated $3NaBH_4$-GdF_3 after the 51st cycle (inset of Fig. 7) shows that the characteristic peaks of $NaBH_4$, GdF_3 and $NaGdF_4$ are clearly observed together with those peaks from residual NaF. Therefore, the capacity drop is attributed to the formation of $NaGdF_4$ and the kinetic delay of partially unconverted NaF, leading to the partial recombination of $NaBH_4$.The $3NaBH_4$-GdF_3 composite retains the cyclic capability up to 51 times, suggesting a dramatic improvement in de-/rehydrogenation performances of $NaBH_4$ through GdF_3 addition. To the best of our knowledge, this is the first time that a successful hydrogen absorption cycling is achieved in a $NaBH_4$-based system over 51 cycles. This implies that the $3NaBH_4$-GdF_3 composite is a promising reversible hydrogen storage system over other previously known borohydride-based systems. Table 2 summaries the cycling properties of some borohydride-based hydrogen storage systems for comparison.

Table 2 Cyclic performances of some borohydride-based hydrogen storage systems.

system	Rehy. Temperature / °C	Rehy. Pressure / MPa	Rehy. Time / h	Cycle number	Ref.
$2LiBH_4$-MgH_2	425	14	12	2	37
$LiBH_4$-TiF_3	350	10	12	1	30
$2LiBH_4$-MgH_2-$0.1NiCl_2$	430	8	-	3	38
LiF-MgB_2	390	6	20	4	26
$LiBH_4$-CaH_2	~ 500	8	12	10	39
$LiBH_4$-C	400	10	2	3	40
$NaBH_4$/C	325	6	5	4	11
2NaH +MgB_2	400	35	24	1	7
$NaBH_4$-GdF_3	180 ~ 400	1 ~ 4	1.6 ~ 10	51	This work

The dependence of rehydrogenation kinetics on pressure and temperature was further analyzed by increasing number of cycles. Clearly, the rehydrogenation rate under 1 MPa (26th, 36th), 2 MPa(27th, 31st, 51st), 3 MPa (28th, 30th) and 4 MPa (29th) initial pressure increases uniformly with pressure at a constant temperature (Fig. S9(b)). Under 4 MPa in the 29th cycle, the capacity of 3.44 wt% H_2 can be still attained within 3 h. While, with increasing the temperature under a constant pressure, the rehydrogenation rate exhibits a gradual increase in the low temperature region and an abrupt increase in the high temperature region (Fig. S9(c)). Rehydrogenation curves under synchronous low-pressure-temperature conditions: 182 °C + 1 MPa, 244 °C + 2 MPa and 400 °C + 4 MPa are also plotted (Fig. S9(d)). It is worth noting that capacities of ~ 0.65 and 1.40 wt% are reached

under 1 MPa at 182 °C (44th), 2 MPa at 244 °C (42nd), respectively, further demonstrating the remarkable reversible sorption performance of $3NaBH_4$-GdF_3 composite, which are not achieved in other light metal borohydride-based binary hydrogen storage composites.

4. Conclusions

In this work, we have systematically investigated the effects of LnF_3 (Ln = La, Ce, Pr, Nd, Sm, Gd, Ho, Er and Yb) on the hydrogen sorption behaviors in $NaBH_4$ by introducing 4 new Ln fluorides - CeF_3, SmF_3, GdF_3 and YbF_3 - into $NaBH_4$. The mechanisms associated with thermodynamic and kinetic modifications in $NaBH_4$ with respect to the LnF_3 addition were correlated with the electronic nature of Ln trivalent cations (*i.e.* electronegativity, electron configurations) and the crystal structures of Ln-B phases. The results reveal that all the studied LnF_3 additives enable the reversible hydrogen sorption in $NaBH_4$ but in different extent. The hydrogen de-/absorption behaviors of the $3NaBH_4$-LnF_3 composites are related to the electron configurations of Ln^{3+} cations. The relationship between rehydrogenation enthalpies of $3NaBH_4$-LnF_3 and the electronegativities of the added Ln^{3+} shows 2 linear correlations with an intersection point at Nd^{3+}. Our results reveal that the $3NaBH_4$-LnF_3 composite with electronegativity of Ln cation lying in the range 1.23 ~ 1.54 is thermodynamically favorable for reversible hydrogen storage. In addition, the unique crystal structure of Ln-B and the geometrical configurations of B in Ln-B crystals facilitate the kinetic recombination of $NaBH_4$. Hydrogen de-/absorption results reveal the best overall promoting effects of GdF_3 on the hydrogen sorption properties of $NaBH_4$ among all the studied LnF_3. In particular, the $3NaBH_4$-GdF_3 composite possesses high cyclic stability over 51 cycles with fast kinetics, and can be rehydrogenated even under 1 MPa H_2 at 182 °C after 44 cycles.

Acknowledgements

Prof. Zou would like to thank the support from the Science and Technology Committee of Shanghai under No. 14JC1491600 and 'Pujiang' project (No. 11PJ1406000). This work is partly supported by Research Fund for the Doctoral Program of Higher Education of China (No. 20100073120007) and from the Shanghai Education Commission (No. 12ZZ017).

References

1 L. Schlapbach and A. Zuttel, *Nature*, 2001, **414**, 353-358.
2 W. Grochala and P. P. Edwards, *Chem. Rev.*, 2004, **104**, 1283-1315.
3 F. Schuth, B. Bogdanovic and M. Felderhoff, *Chem. Commun.*, 2004, 2249-2258.
4 S. V. Alapati, J. K. Johnson and D. S. Sholl, *J. Phys. Chem. B*,2006, **110**, 8769-8776.
5 http://www1.eere.energy.gov/hydrogenandfuelcells/pdfs/freedomcar_targets_explanations.pdf
6 P. Martelli, R. Caputo, A. Remhof, P. Mauron, A. Borgschulte and A. Zuttel, *J. Phys. Chem. C*, 2010, **114**, 7173-7177.
7 G. Barkhordarian, T. Klassen, M. Dornheim and R. Bormann, *J. Alloys Compd.*, 2007, **440**,L18-L21.
8 Y. Nakamori, K. Miwa, A. Ninomiya, H. Li, N. Ohba, S.-i. Towata, A. Züttel and S.-i. Orimo, *Phys. Rev. B*, 2006, **74**, 045126.
9 D. Ravnsbaek, Y. Filinchuk, Y. Cerenius, H. J. Jakobsen, F. Besenbacher, J. Skibsted and T. R. Jensen, *Angew. Chem. Int. Ed.*, 2009, **48**, 6659-6663.
10 G. Xia, Q. Gu, Y. Guo and X. Yu, *J. Mater. Chem.*, 2012, **22**, 7300-7307.
11 P. Ngene, R. van den Berg, M. H. W. Verkuijlen, K. P. de Jong and P. E. de Jongh, *Energy Environ. Sci.*, 2011, **4**, 4108-4115.
12 J. F. Mao, Z. P. Guo, I. P. Nevirkovets, H. K. Liu and S. X. Dou, *J. Phys. Chem. C*, 2012, **116**, 1596-1604.
13 J. J. Vajo, S. L. Skeith and F. Mertens, *J. Phys. Chem. B*, 2005, **109**, 3719-3722.
14 S. -A. Jin, J. -H. Shim, Y. W. Cho, K. -W. Yi, O. Zabara and M. Fichtner, *Scr. Mater.*, 2008, **58**, 963-965.
15 L. N. Chong, J. X. Zou, X. Q. Zeng and W. J. Ding, *J. Mater. Chem. A*, 2013, **1**, 3983-3991.
16 L. N. Chong, J. X. Zou, X. Q. Zeng and W. J. Ding, *J. Mater. Chem. A*,2013, **1**,13510-13523.
17 L. N. Chong, J. X. Zou, X. Q. Zeng and W. J. Ding, *J. Mater. Chem. A*, 2014, **2**, 8557-8570.
18 L. N. Chong, J. X. Zou, X. Q. Zeng and W. J. Ding, *Int. J. Hydrogen Energy*, 2014, **39**, 14275-14281.
19 S. V. Meschel and O. J. Kleppa, *J. Alloys Compd.*, 1995, **226**, 243-247.
20. J. E. Olsen, C. Frommen,T. R. Jensen, M. D. Riktor, M. H. Sørby and B. C. Hauback, *RSC Adv.*, 2014, **4**, 1570-1582.
21. M. B. Ley, S. Boulineau, R. Janot, Y. Filinchuk and T. R. Jensen, *J. Phys. Chem. C*, 2012, **116**, 21267-21276.
22 H. E. Kissinger, *Anal. Chem.*, 1957, **29**, 1702-1706.
23 I. K. Fidelis and T. J. Mioduski, *Struct. Bond.*,1981,**47**, 27-51.
24. U. Mirsaidov, *Int. J. Hydrogen Energy*, 2011, **36**, 1190-1191.
25 A. Roine, *Outokumpu HSC Chemistry for Windows: Chemical Reaction and Equilibrium Software with Extensive Thermodynamical Database and Flowsheet Simulation, Version 5.1*,02103-ORC-T, Outokumpu Research Oy, Finland, 2002.
26 R. Gosalawit-Utke, J. M. Bellosta von Colbe, M. Dornheim, T. R. Jensen, Y. Cerenius, C. B. Minella, M. Peschke and R. Bormann, *J. Phys. Chem. C*, 2010, **114**, 10291-10296.
27 T. Nagaki, Y. Inoue, I. Kojima and I. Yasumori, *J. Phys. Chem.*, 1980, **84**, 1919 -1925.
28 T. Yorisaki, A. Tillekaratne, Q. Ge, C. Oshima, S. Otani and M. Trenary, *Surf. Sci.*, 2009, **603**, 3011-3020.
29 I. J. Kang and C. H. Park, *J. Korean Phys. Soc.*, 2006, **49**, S490-S494.
30 Y. H. Guo, X. B. Yu, L. Gao, G. L. Xia, Z. P. Guo and H. K. Liu, *Energy Environ. Sci.*, 2010, **3**, 465-470.
31 J. Yang, A. Sudik and C. Wolverton, *J. Phys. Chem. C*, 2007, **111**, 19134-19140.
32 M. L. Christian and K.-F. Aguey-Zinsou, *Acs Nano*, 2012, **6**, 7739-7751.
33 J.-H. Shim, J.-H. Lim, S.-u. Rather, Y.-S. Lee, D. Reed, Y. Kim, D. Book and Y. W. Cho, *J. Phys. Chem. Lett.*, 2010, **1**, 59–63.
34 J. X. Zou, L. J. Li, X. Q. Zeng and W. J. Ding, *Int. J. Hydrogen Energy*, 2012, **37**, 17118-17125.
35 K. y. Li and D. f. Xue, *J. Phys. Chem. A*, 2006, **110**, 11332-11337.
36 C. Bonatto Minella, S. Garroni, C. Pistidda, R. Gosalawit-Utke, G. Barkhordarian, C. Rongeat, I. Lindemann, O. Gutfleisch, T. R. Jensen, Y. Cerenius, J. Christensen, M. D. Baró, R. d. Bormann, T. Klassen and M. Dornheim, *J. Phys. Chem. C*, 2011, **115**, 2497-2504.
37 R. Gosalawit−Utke, T. K. Nielsen, K. Pranzas, I. Saldan, C. Pistidda, F. Karimi, D. Laipple, J. Skibsted, T. R. Jensen, T. Klassen and M. Dornheim, *J. Phys. Chem. C*, 2012, **116**, 1526-1534.
38 J. Shao, X. Z. Xiao, L. X. Chen, X. L. Fan, S. Q. Li, H. W. Ge and Q. D. Wang, *J. Mater. Chem.*, 2012, **22**, 20764-20772.
39 J.-H. Lim, J.-H. Shim, Y.-S. Lee, J.-Y. Suh, Y. W. Cho and J. Lee, *Int. J. Hydrogen Energy*, 2010, **35**, 6578-6582.
40 J. J. Vajo and G. L. Olson, *Scr. Mater.*, 2007, **56**, 829-834.